Transition paths of North Atlantic Deep Water

Philippe Miron
Center for Ocean-Atmospheric Prediction Studies
Florida State University
Tallahassee, FL, USA

F. J. Beron-Vera[*]
Department of Atmospheric Sciences
Rosenstiel School of Marine and Atmospheric Science
University of Miami, Miami, FL, USA

M. J. Olascoaga
Department of Ocean Sciences
Rosenstiel School of Marine and Atmospheric Science
University of Miami, Miami, FL, USA

May 25, 2022

Abstract

Recently introduced in oceanography to interpret the near surface circulation, *Transition Path Theory* (*TPT*) is a methodology that rigorously characterizes ensembles of trajectory pieces flowing out from a source last and into a target next, i.e., those that most productively contribute to transport. Here we use TPT to frame, in a statistically more robust fashion than earlier analysis, equatorward routes of North Atlantic Deep Water (NADW) in the subpolar North Atlantic. TPT is applied on all available RAFOS and Argo floats in the area by means of a discretization of the Lagrangian dynamics described by their trajectories. By considering floats at different depths, we investigate transition paths of NADW in its upper (UNADW) and lower (LNADW) layers. We find that the majority of UNADW transition paths sourced in the Labrador and southwestern Irminger Seas reach the western side of a target arranged zonally along the southern edge of the subpolar North Atlantic domain visited by the floats. This is accomplished in the form of a well-organized deep boundary current (DBC). LNADW transition paths sourced west of the Reykjanes Ridge reveal a similar pattern, while those sourced east of the ridge are found to hit the western side of the target via a DBC and also several other places along it in a less organized fashion, indicating southward flow along the eastern and western flanks of the Mid-Atlantic Ridge. Naked-eye inspection of trajectories suggest generally much more diffusive equatorward NADW routes. A source-independent dynamical decomposition of the flow domain into analogous backward-time basins of attraction, beyond the reach of direct inspection of trajectories, reveals a much wider influence of the western side of the target for UNADW than for LNADW. For UNADW, the average expected duration of the pathways from the Labrador and Irminger Seas was found to be of 2 to 3 years. For LNADW, the duration was found to be influenced by the Reykjanes Ridge, being as long as 8 years from the western side of the ridge and of about 3 years on average from its eastern side.

---

[*]Email address for correspondence: fberon@miami.edu

1 Introduction

The North Atlantic Deep Water (NADW) formed in the Labrador and Nordic Seas has historically been depicted as flowing equatorward, out of the subpolar North Atlantic in the form of a well-defined deep western boundary current (WDBC) (Stommel, 1958). This WDBC constitutes the deep limb of the Atlantic Meridional Overturning Circulation, a conduit for carbon, heat, and freshwater, acquired at the sea surface (Sabine and Tanhua, 2010). This traditional view of the deep circulation has been challenged by Lagrangian observations and simulations (Lozier et al., 2013; Bower et al., 2019). The paths of NADW in its upper layer or UNADW (Lavender et al., 2000, 2005; Fischer and Schott, 2002; Bower et al., 2009, 2019; Lozier et al., 2013) and, particularly, in its lower layer or LNADW (Zou et al., 2020, 2017) appear to exhibit more dispersion than originally believed.

This paper aims to scrutinize the spread of NADW more deeply than precedent analyses via the application of *Transition Path Theory* (*TPT*) (E and Vanden-Eijnden, 2006; Vanden-Eijnden, 2006; Metzner et al., 2006; E and Vanden-Eijnden, 2010), a methodology that has been very recently brought to oceanography, for the interpretation of near surface circulation (Miron et al., 2021; Drouin et al., 2012). We will specifically apply TPT on all available satellite-tracked profiling Argo float data and acoustically-tracked RAFOS float data, including those collected during the Overturning in the Subpolar North Atlantic Program (OSNAP) (Susan Lozier et al., 2017). TPT will allow us to make several quantitative assessments of the spread of NADW which lie beyond the reach of, or are difficult to frame using, conventional Lagrangian ocean analysis tools. These include:

1. quantifying the extent by which UNADW and LNADW flow equatorward in the form of WDBCs;

2. estimating the averaged time taken by UNADW and LNADW to exit the subpolar North Atlantic from any location within; and

3. dynamically decomposing the flow domain into analogous backward-time basins of attraction for UNADW and LNADW.

This is all possible because TPT seeks to frame the tracer trajectories that statistically most effectively contribute to the transport from one region of the flow domain, or *source*, to another region, or *target*. Such *transition paths* are formed by trajectory pieces that connect source and target in such a way that *each trajectory piece comes out of the source last and goes to the target next*. In other words, TPT unveils from typically highly convoluted trajectories those portions that most productively contribute to transport. More specifically, TPT provides rigorous means for expressing various statistics of the ensemble of transition pathways. These include:

1. the bottlenecks during the transitions;

2. the most likely transition channels;

3. the rate of reactive trajectories leaving a source or entering a target; and

4. the mean duration of reactive trajectories.

The modeling framework for TPT analysis is provided by an autonomous, discrete-time Markov chain (Brémaud and Norris, 1975), which has been successfully used to investigate long-time asymptotics in Lagrangian ocean dynamics (Maximenko et al., 2012; Froyland et al., 2014; Miron et al., 2017; Olascoaga et al., 2018; Beron-Vera et al., 2020; Miron et al., 2019a,b, 2021; Drouin et al., 2012). By combining available short-run trajectories pieces, time-homogeneous Markov chain modeling is particularly useful when dealing with observed trajectory records, which are of finite-time nature. In the present case, in particular, a limited amount of float trajectories connect the various source and target sets considered to attempt a direct assessment of productive transport.

The rest of this paper is organized as follows. We begin in Sec. 22.1 with the mathematical setup for Markov chain modeling, followed by a self-contained exposition of the main results of TPT. In Sec. 22.2 we describe the construction of the Markov chain models proposed for the evolution of the UNADW and LNADW components of NADW using observed float data at appropriate depths. The choice of source and target sets for TPT analysis is rationalized in Sec. 22.3. The results from the TPT analysis are presented in Sec. 3. These are discussed in light of results from other analyses in Sec. 4. Finally, Sec. 5 offers a summary and the conclusions.

2   Methods

2.1   Transition path theory

Let χ_n denote random position at discrete time $nT \geq 0$, $n \in \mathbb{Z}_0^+$, on a closed two-dimensional flow domain D covered by nonoverlapping boxes $\{b_1, \ldots, b_N\}$. Given $\mathrm{prob}(\chi_n \in b_i)$, we assume $\mathrm{prob}(\chi_{n+1} \in b_j) = \sum_i P_{ij} \mathrm{prob}(\chi_n \in b_i)$, where

$$P_{ij} := \mathrm{prob}(\chi_1 \in b_j \mid \chi_0 \in b_i) \tag{1}$$

is the one-step conditional probability of transitioning between b_i and b_j. Note that $\sum_j P_{ij} = 1$, so $\mathsf{P} = (P_{ij}) \in \mathbb{R}^{N \times N}$, called a *transition matrix*, is (row) stochastic. Let $x(t)$ represent a very long float trajectory visiting every box of the covering of D many times. In practice, there are many finite-length float trajectories that sample D well. Let $x(t)$ and $x(t+T)$ at any $t > 0$ provide observations for χ_0 and χ_1, respectively. These are used to approximate P_{ij} via transition counting, viz.,

$$P_{ij} \approx \frac{C_{ij}}{\sum_k C_{ik}}, \quad C_{ij} := \#\{x(t) \in b_i, \, x(t+T) \in b_j, \, t : \mathrm{any}\}. \tag{2}$$

In other words, the float motion is envisioned as that of random walkers along an autonomous, discrete-time *Markov chain* (cf., e.g., Brémaud and Norris, 1975). At the continuous level, the Lagrangian dynamics as described by the float trajectories are assumed to obey a time-homogeneous stochastic (i.e., steady-advection–diffusion) process. i The chain will be assumed to be *ergodic* (i.e., such that all its states (boxes of the covering of D) communicate irrespective of the starting state) and *mixing* (i.e., such that none of its states is revisited cyclically). In these conditions, eigenvalue one of P is both maximal and simple. The corresponding *left* eigenvector, $\boldsymbol{\pi} = (\pi_i) \in \mathbb{R}^{1 \times N}$, can be chosen componentwise positive, and is both invariant and limiting, i.e., $\boldsymbol{\pi} = \boldsymbol{\pi}\mathsf{P} = \lim_{n \uparrow \infty} \mathbf{f}\mathsf{P}^n$ for any $\mathbf{f} \in \mathbb{R}^{1 \times N}$. Normalized to a *probability* vector (i.e., so $\sum_i \pi_i = 1$), $\boldsymbol{\pi}$ represents a *stationary distribution*, which will be assumed to set the long-time asymptotics of $\{\chi_n\}$, namely, $\mathrm{prob}(\chi_n \in b_i) = \pi_i$. This will allow us to investigate generic aspects of the float motion in statistical stationarity, rather than particular aspects bound to initial conditions.

The TPT of E and Vanden-Eijnden (2006) provides a rigorous approach to study transitions from a set $A \subset D$ to another, disjoint set $B \subset D$. The pieces of trajectories running from A, referred to as *source*, to B, referred to as *target*, without going back to A or going through B in between, are the main focus and known as *reactive trajectories* (Fig. 1). This uses traditional jargon that identifies source set A with the reactant of a chemical transformation and target set B with its product. Reactive trajectories are also known as *transition paths*; will use this terminology or similar to refer to them here too. Most importantly, they describe pathways that *contribute most effectively to the transport from A to B*. For the problem of interest, transition *float* paths from a set A within the subpolar gyre to a set B located at its southern edge will highlight the most effective export paths of the deep water masses sampled by the floats.

The main objects of TPT are the *forward*, $\mathbf{q}^+ = (q_i^+) \in \mathbb{R}^{1 \times N}$, and *backward*, $\mathbf{q}^- = (q_i^-) \in \mathbb{R}^{1 \times N}$, *committor probabilities*. These give the probability of a random walker initially in b_i to first enter B and last exit A, respectively. Namely, $q_i^{\pm} := \mathrm{prob}(\tau_B^{\pm} < \tau_A^{\pm} \mid \chi_0 \in b_i)$, where $\tau_S^{\pm} := \inf\{nT : \chi_{\pm n} \in S\}$ with the plus (resp., minus) sign denoting *first entrance* (resp., *last exit*) *time* of a set $S \subset D$. The committors are fully computable from P and $\boldsymbol{\pi}$, since $\mathrm{prob}(\chi_n \in b_i) = \pi_i$, according to:

$$q_i^{\pm} = \sum_j P_{ij}^{\pm} q_j^{\pm}, \, i \in \overline{A \cup B}, \quad q_{i \in A}^{\pm} = \delta_{1 \mp 1, 2}, \quad q_{i \in B}^{\pm} = \delta_{1 \pm 1, 2}. \tag{3}$$

Here, $\mathsf{P}^+ = \mathsf{P}$, $P_{ij}^- := \mathrm{prob}(\chi_0 = j \mid \chi_1 = i) = \frac{\pi_j}{\pi_i} P_{ji}$ are the entries of the *time-reversed* transition matrix, i.e., for the original chain traversed in backward time, $\{\chi_{-n}\}$; the overbar means complement; and the short-hand notation $i \in S$ for $i : b_i \subset S$ is herein used.

The committor probabilities are used to express several statistics of the ensemble of reactive trajectories as follows (e.g., Metzner et al., 2006; Helfmann, 2020).

1. The *distribution of reactive trajectories*, $\boldsymbol{\mu}^{AB} = (\mu_i^{AB}) \in \mathbb{R}^{1 \times N}$, where μ_i^{AB} is defined as the joint probability that a trajectory is in box b_i while transitioning from A to B and is computable as

$$\mu_i^{AB} = q_i^- \pi_i q_i^+, \tag{4}$$

    describes the bottlenecks during the transitions, i.e., where reactive trajectories spend most of their time. Clearly, $\mu_{i \in A \cup B}^{AB} \equiv 0$.
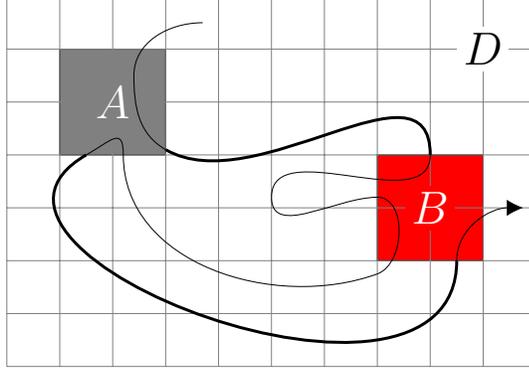
Figure 1: Schematic representation of a piece of a hypothetical infinitely long float trajectory (black) that densely, albeit not necessarily uniformly, fills a closed flow domain D, partitioned into boxes (black). Indicated in gray and red respectively are source (A) and target (B) sets. Highlighted by the thick (black) lines are two members of an ensemble of reactive trajectories. These are the trajectory subpieces that connect the boundary of A with the boundary of B in direct transition from A to B, i.e., without returning back to A or going through B in between.

2. The *effective current of reactive trajectories*, $\mathsf{f}^+ = (f_{i,j}^+) \in \mathbb{R}^{N \times N}$, where $f_{i,j}^+$ gives the net flux of trajectories going through b_i at time nT and b_j at time $(n+1)T$ on their way from A to B, indicates the most likely transition channels. This is computable according to

$$f_{ij}^+ = \max\left\{f_{ij}^{AB} - f_{ji}^{AB}, 0\right\}, \quad f_{ij}^{AB} = (1 - \delta_{ij})q_i^- \pi_j P_{ij} q_j^+. \tag{5}$$

To visualize reactive trajectories, one can proceed in two different but complementary ways, as we do here.

(a) On one hand, one can simply depict the magnitude and the direction of the effective reactive current f^+ out of each box b_i of the flow domain covering. This is done by attaching to each b_i the two-dimensional vector on the "plane" $\sum_{j \neq i} f_{ij}^+ \vec{e}_{ij}$, where $\vec{e}_{ij} \in \mathbb{R}^{2 \times 1}$ is the unit vector *pointing from the center of box b_i to the center of b_j* (Helfmann, 2020; Miron et al., 2021).

(b) On the other hand, one can depict *dominant transition paths*, which maximize the minimal effective current along the reactive trajectories (Metzner et al., 2009). The larger the minimal effective current along a reactive trajectory, the more current it conducts from A to B. In practice one applies a flow decomposition algorithm that seeks to concatenate "bottlenecks" in associated f^+-weighted directed graphs, i.e., edges with minimal effective current (cf. Metzner et al., 2009, for details). Dominant transition *float* paths between appropriately chosen source and target sets will unveil the major deep water mass parcel pathways connecting them most productively.

3. The *rate of reactive trajectories* leaving A or entering $\tilde{B} \subseteq B$, defined respectively as the probability per time step of a reactive trajectory to leave A or enter $\tilde{B} \subseteq B$, are computed respectively as

$$k^{A \to} = \sum_{i \in A, j} f_{ij}^{AB}, \quad k^{\tilde{B} \leftarrow} = \sum_{i, j \in \tilde{B}} f_{ij}^{AB}, \tag{6}$$

and can be interpreted in various ways. One is as the proportion of reactive trajectories leaving A or entering $\tilde{B} \subseteq B$. If divided by T, the other possible interpretation is as the frequency at which a reactive trajectory leaves A or enters $\tilde{B} \subseteq B$. In particular, $k^{A \to} \equiv k^{B \leftarrow}$. Moreover, in a fully three-dimensional calculation, with three-dimensional boxes rather than "tiles" as considered in the present two-dimensional analysis constrained by the data availability, reactive rates can be interpreted as volumetric flow rates. More specifically, upon dividing $k^{A \to}$ or $k^{\tilde{B} \leftarrow}$ by T and multiplying the result by the volume spanned by the box covering of D, one would get the volumetric flow rate out of A or into $\tilde{B}$, respectively.

4. Finally, the *expected duration*, t^{AB}, of a transition from A to B is obtained by dividing the probability of being reactive by the transition rate interpreted as a frequency, viz.,

$$t^{AB} = \frac{\sum_{j \in \overline{A \cup B}} \mu_j^{AB}}{k^{AB}}. \tag{7}$$

When D represents an open flow domain, i.e., with trajectories flowing out and returning back in as is the case of this work, P is no longer stochastic, which requires an adaptation of TPT (Miron et al., 2021). This involves augmenting chain P by a stochastic transition matrix $\tilde{\mathsf{P}} \in \mathbb{R}^{(N+1) \times (N+1)}$ defined by

$$\tilde{\mathsf{P}} := \begin{pmatrix} \mathsf{P} & \mathbf{p}^{D \to \omega} \\ \mathbf{p}^{D \leftarrow \omega} & \mathbf{0} \end{pmatrix} \tag{8}$$

where ω is the state, called a *two-way nirvana state*, used to augment the chain defined by P. In eq. (8), vector $\mathbf{p}^{D \to \omega} := \left(1 - \sum_{j \in D} P_{ij}\right)^{\top} \in \mathbb{R}^{N \times 1}$ gives the outflow from D and the *probability* vector $\mathbf{p}^{D \leftarrow \omega} \in \mathbb{R}^{1 \times N}$ gives the inflow. When possible, this is estimated from the trajectory data. Other possibilities exist, for instance when there are not enough trajectory observations or their limited length prevents them from capturing the return flow, as is for example the case with the deepest floats analyzed in this study. One such possibility is redistributing any imbalance like the *quasi*stationary distribution $\boldsymbol{\pi}$, normalized by $\sum_i \pi_i$, or uniformly along the chain. However, the TPT results of this paper were not found sensitive to any of these choices. The expectation is that the dynamics produced by the restriction of $\tilde{\mathsf{P}}$ to D, $\tilde{\mathsf{P}}|_D$, is consistent with the original dynamics, i.e., produced by P, under the assumption of well-mixedness between exit from D and reentry into it. TPT is adapted in Miron et al. (2021) such that transitions between A and B are constrained to take place within D, i.e., they avoid ω. This is accomplished by replacing $\boldsymbol{\pi}$ in the TPT formulae above by $\tilde{\boldsymbol{\pi}}|_D$, where $\tilde{\boldsymbol{\pi}}$ is the stationary distribution of $\tilde{\mathsf{P}}$.

We finalize this section by noting that, theoretically, by ergodicity of a Markov chain, the TPT statistics can be computed by "counting" transition events of an infinitely long, $\boldsymbol{\pi}$-distributed trajectory (Vanden-Eijnden, 2006; Helfmann, 2020). For instance, the forward committor q_i^+ is equal to the fraction of all visits paid by such a trajectory to box b_i after having directly transitioned to B without hitting A first. One may then wonder why all the TPT sophistication is really necessary when one could simply do an approximation by counting. The answer is in the nature of the trajectory data: sufficiently many trajectories that are sufficiently long and appropriately distributed would be needed to resolve the transition statistics. None of these conditions are satisfied in practice, not even if the trajectory data are generated numerically, and the best available option is to combine all available trajectory information into a Markov chain.

2.2 Construction of the Markov chain model(s)

The Markov chain is constructed using trajectories from Argo and RAFOS floats deployed in, or travelling through, the subpolar North Atlantic above 40°N. In this region, the inclusion of Argo floats is critical to the analysis of the NADW circulation due to the insufficient density of RAFOS floats, which drift at a constant depth. Given the nature of Argo floats, which surface from their parking depth every ten days, we note that surface currents account on average for 15% of Argo float displacement. Since 2013, the majority of Argo floats use the Iridium telecommunications service, which allows for faster transmission, decreasing the time period at the surface, as well as the influence of surface currents on the float trajectory. On the other hand, in Miron et al. (2019a) it was shown that the vertical excursions of the Argo floats do not substantively affect the description of the Lagrangian motion at their parking depth. Thus we proceed with confidence and consider Argo and RAFOS floats together in the analysis.

The Argo floats deployed in the Labrador Sea during the World Ocean Circulation Experiment and the Deep Convection Experiment in the 1990s, and elsewhere since the 1980s, encompass most (1513 of a total of 2339 floats) of the data record (Fig. 2). The OSNAP program contributes to the data record over the period 2014–2017 with 134 RAFOS floats, deployed in various locations of the subpolar North Atlantic. There are 1745 floats sampling depths between 750 and 1500 m, and 302 floats between 1800 and 3500 m. Observational trajectories in these two depth ranges are here used to construct two independent Markov chains, describing the evolution of the UNADW and LNADW components of NADW, respectively. The construction of the two Markov chains first involves covering each region D sampled by each set of trajectories, with a grid of $0.6° \times 0.6°$ boxes. Henceforth, we differentiate between the shallow Markov chain, describing the circulation of UNADW (Fig. 3, left panel) and the deep Markov chain, describing the circulation of LNADW (Fig. 3, right panel). The area of the boxes is not uniform due to the Earth's sphericity, but this is of no consequence if the discretization of the Lagrangian dynamics is carried out appropriately; cf. Miron et al. (2019a). To compute

the transition matrix P of each Markov chain, we use the float positions at any time t and $T = 10\,\text{days}$ later to provide observations of random positions χ_0 and χ_1. The transition time ($T = 10\,\text{days}$) is sufficiently long to guarantee negligible memory into the past (we have estimated a Lagrangian decorrelation time of about 5 days) so the Markov assumption can be expected to approximately hold. This T choice also guarantees sufficient communication among boxes, while still maximizing sampling. The results presented below, however, are insensitive to T choices between 5 days to 20 days. Similar results were found earlier by Miron et al. (2019a) using RAFOS and Argo float data in the Gulf of Mexico.

An important cautionary note is that UNADW and LNADW are usually defined by their (mass) density signature rather than depth ranges. Commonly considered sigma-potential density ranges are 27.66–27.8 and 27.8–27.88 kg m^{-3}, respectively (Lozier et al., 2019). These respectively lie, typically, within the depth ranges 750–1500 m and 1800–3500 m (discarding data between 1500–1800 m near their interface) here used to differentiate between the two water masses in question. Their choice had the above observation in mind, but it was also constrained by the data availability. Thus our NADW flow description admittedly is an approximation.
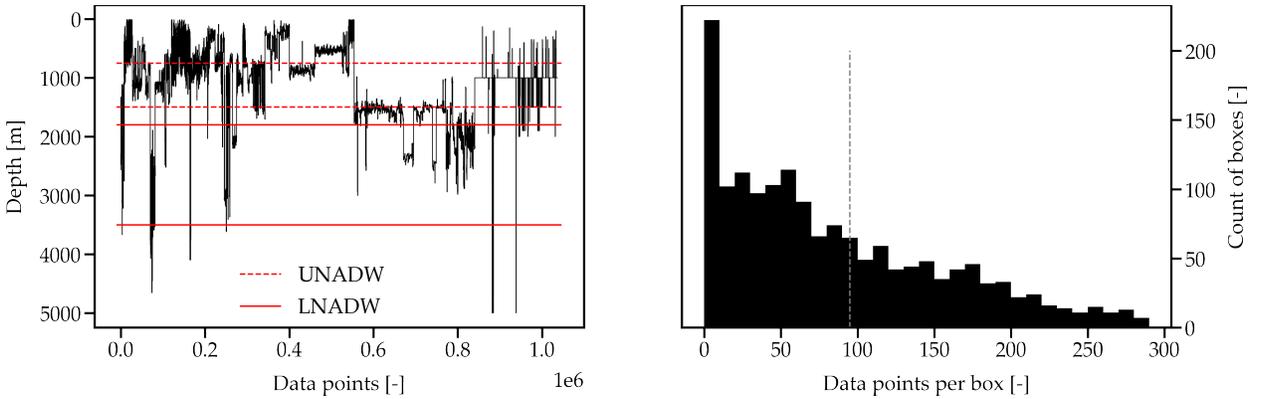

Figure 2: (left) Independent of horizontal position or time, depth reached by each RAFOS or Argo float deployed in, or traversing the, subpolar North Atlantic (Fig. 3) since the 1980s. The broken red lines indicate the limits of the depth ranges chosen to construct the Markov chains that represent the motion of the UNADW (750–1500 m) and LNADW (1800–3500 m) components. (right) Histogram of the raw data density within boxes of the domain (above 50°N) with the broken gray line indicating the average value of 95 data points per box. Replace the right panel to include an histogram of the data density.

2.3 Source and target sets for TPT analysis

Two source sets, A_1 and A_2, and a single target set B, given by the union of nearly contiguous boxes, are defined for each of the two Markov chains (Fig. 3). For the UNADW chain (Fig. 3, top panel), sets A_1, positioned in the middle of the Labrador Sea, and A_2, located in the southwestern Irminger Sea off the southern tip of Greenland. For the LNADW chain (Fig. 3, bottom panel), sets A_1 and A_2 straddle the Reykjanes Ridge. The UNADW sources in the Labrador Sea and the southwestern Irminger Sea lie in regions of presumed deep water formation (Pickart et al., 2003). The southwestern Irminger Sea and the LNADW sources overlap with the location of an OSNAP mooring array or coincide with the release sites of RAFOS floats (Ramsey et al., 2020). In particular, the LNADW source east of the Reykjanes Ridge can be expected to intersect Iceland–Scotland Overflow Water. Constrained by the availability of data and the depth of the water masses across the North Atlantic, the target set B is taken to represent the *southern edge* of the subpolar North Atlantic, so the TPT analysis enables assessing pathways of NADW out of it (Fig. 3). For the UNADW chain, which has a higher density of float data, this crosses the domain at a latitude of 50°N. For the LNADW chain, for which the float coverage is poorer, it is positioned approximately along 51°N. Note that each set B includes a meridional set of boxes along 35°N extending out to the Charlie–Gibbs Fracture Zone (CGFZ), at about 53°N. This set of target boxes is included to assess internal pathways in the subpolar North Atlantic.
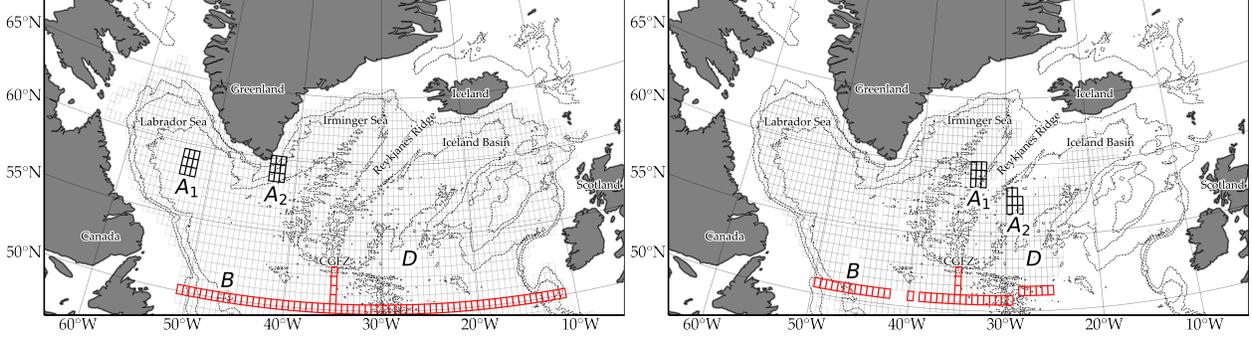
Figure 3: Box (gray) of the subpolar North Atlantic regions defining the UNADW (left) and LNADW (right) Markov chain models, constructed using float data within 750–1500 m and 1800-3500 m, respectively. Source and target sets for TPT analysis are indicated in black and red, respectively. Isobaths 1000 m, 2000 m and 3000 m are shown in this and in all subsequent figures for reference.

3 Results

3.1 Transition pathways of UNADW

We begin by discussing the structure of the UNADW forward ($\mathbf{q}^+$) and backward ($\mathbf{q}^-$) committor probabilities; cf. eq. (3). These are shown in the left and right panels of Fig. 4, with the source placed in the Labrador (top) and southwestern Irminger (bottom) Sea. The probability of the trajectories to commit to the target in forward time increases toward the target. Similarly, their probability to commit in backward time to the source increases toward the source. By construction, the forward committor vanishes at the source and is maximal at the target, and vice versa for the backward committor. Clearly, there is no reactive current inside the source and the target, where $q_i^+ = 0$ and $q_i^- = 0$ for each box b_i covering these sets, respectively, and it will be small in regions covered by boxes where $q_i^+ \approx 0$ *or* $q_i^- \approx 0$. This takes place in most of the eastern subpolar North Atlantic (Fig. 5).
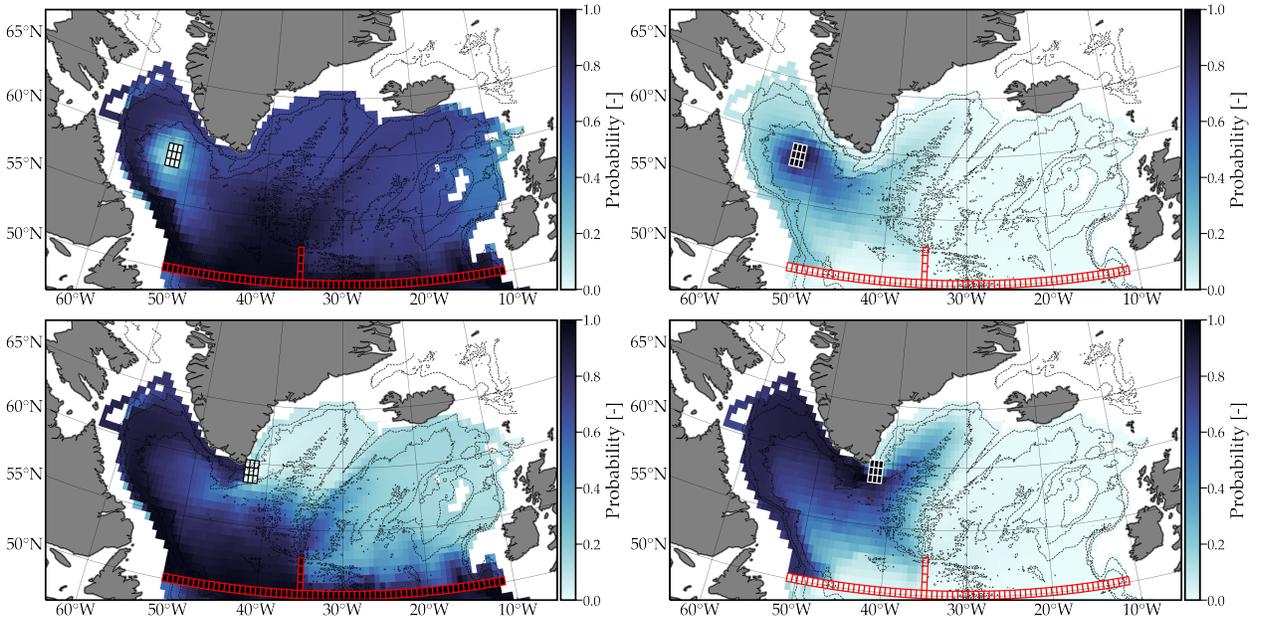

Figure 4: (top) For the UNADW Markov chain model with the source in the Labrador Sea, probability of trajectories to commit to the target (red boxes) in forward time (left) and to the source (black/white boxes) in backward time (right). (bottom) As in the top panels, but with the source in the Irminger Sea.

More specifically, in the left and right panels of Fig. 5 the resulting effective reactive currents of UNADW are depicted alongside their associated dominant transition paths, with the top and bottom rows corresponding to the Labrador and Irminger Sea sources, respectively. The dominant transition paths are colored according to the minimal effective reactive current along their path.
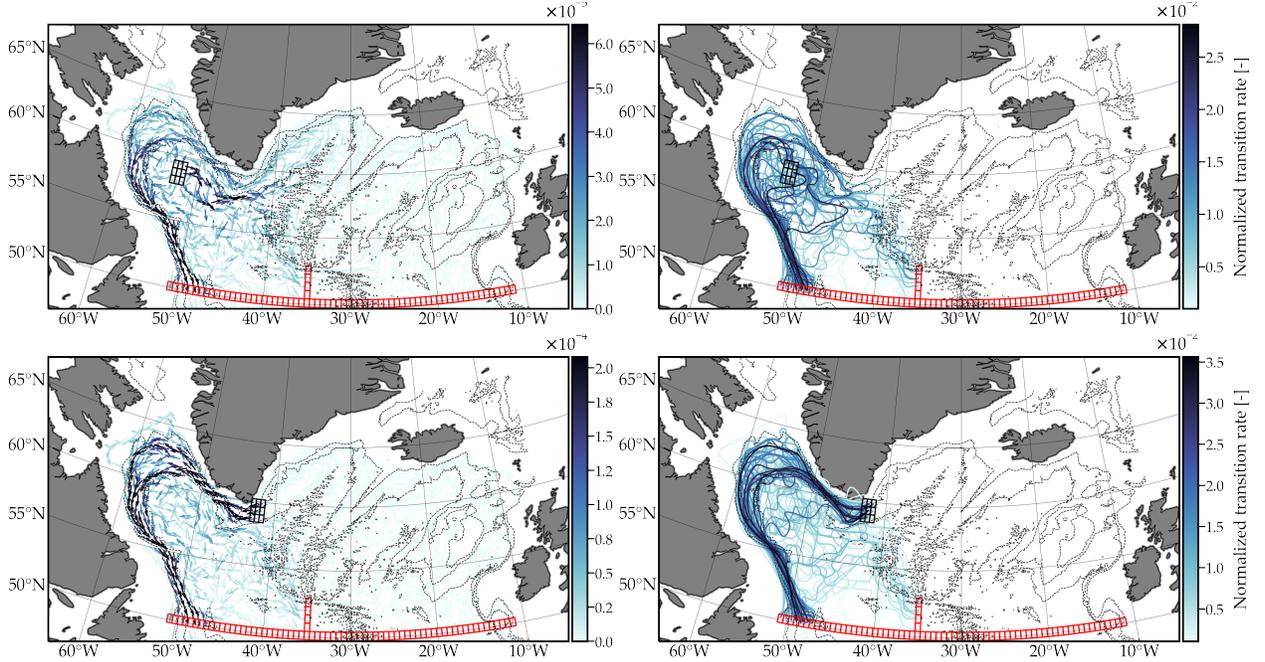

Figure 5: (top) For the UNADW chain with the source in the Labrador Sea, effective reactive currents (left) and dominant transition paths accounting for 90% of the probability flux of reactive trajectories (right). (bottom) As in the top panels, but with the source in the Irminger Sea.

As expected from the analysis of the committors, most of the reactive transitions of UNADW take place in the western subpolar North Atlantic. From both sources, the majority of the transition pathways reach the target at its western edge along a well-defined DBC, seemingly consistent with f/h conservation, where f is the Coriolis frequency and h is depth (LaCasce and Bower, 2000).

For UNADW emerging from the source centered in the Labrador Sea (Fig. 5 top), a sizeable amount of reactive current is initially directed eastward, into the Irminger Sea, where it reaches the East Greenland Current and flow around Greenland. Dominant pathways (top-right panels, accounting for 90% of the probability flux of reactive trajectories) emerging from the Labrador Sea show some degree of isotropicity, consistent with f/h conservation in a region where the bottom topography is relatively flat. The majority of dominant paths eventually join to form a WDBC, and swiftly reach the southwestern edge of the domain. In addition, some interior transition paths are seen to connect the Labrador Sea source with the meridional of boxes of the target at 35°W, indicating possible transition pathways of UNADW connecting the western and eastern subpolar North Atlantic through the CGFZ, previously identified by Lavender et al. (2000, 2005) and more recently quantified by Gonçalves Neto et al. (2020). From the Labrador Sea, such internal paths represent a small percentage, not exceeding 10%, of the total amount of transitions between the Labrador Sea source and the target.

For UNADW emerging from the southwestern Irminger Sea source (Fig. 5 bottom), the DBC is restricted between the 1000- and 3000-m isobaths as it progress northwestward bordering western Greenland. At about 61°N where the 2000- and 3000-m isobaths separate from one another, the reactive current splits into two branches, one roughly following the 3000-m isobath and another one following the 2000-m isobath very closely. The two branches eventually merge, roughly off the northeastern end of the Labrador Peninsula, where the 2000- and 3000-m isobaths get closer again, into a single-branch DBC that flows out of the subpolar North Atlantic. The two UNADW paths inferred by the TPT analysis are hard to reveal from the inspection of individual float trajectories. The two DBC branches unveiled by TPT provide observational support to inferences made from the analysis of simulated float trajectories (de Jong et al., 2016) as well as robust

statistical confirmation of earlier inferences made from the inspection of a subset of the float data considered here (Cuny et al., 2016).

3.2 Transition pathways of LNADW

The left and right panels of Fig. 6 show $\mathbf{q}^+$ and $\mathbf{q}^-$, respectively, with the source of the LNADW chain placed west (top) and east (bottom) of the Reykjanes Ridge. Similarly to the UNADW chain, $q_i^- \approx 0$ in boxes covering most of the eastern and the interior of the subpolar North Atlantic when the source is placed west of the Reykjanes Ridge. LNADW transition currents out of that source will necessary be small. When the source is placed east of the Reykjanes Ridge, $q_i^- \approx 0$ everywhere in the subpolar North Atlantic domain, except in the West European Basin, where reactive currents can be expected to concentrate in.
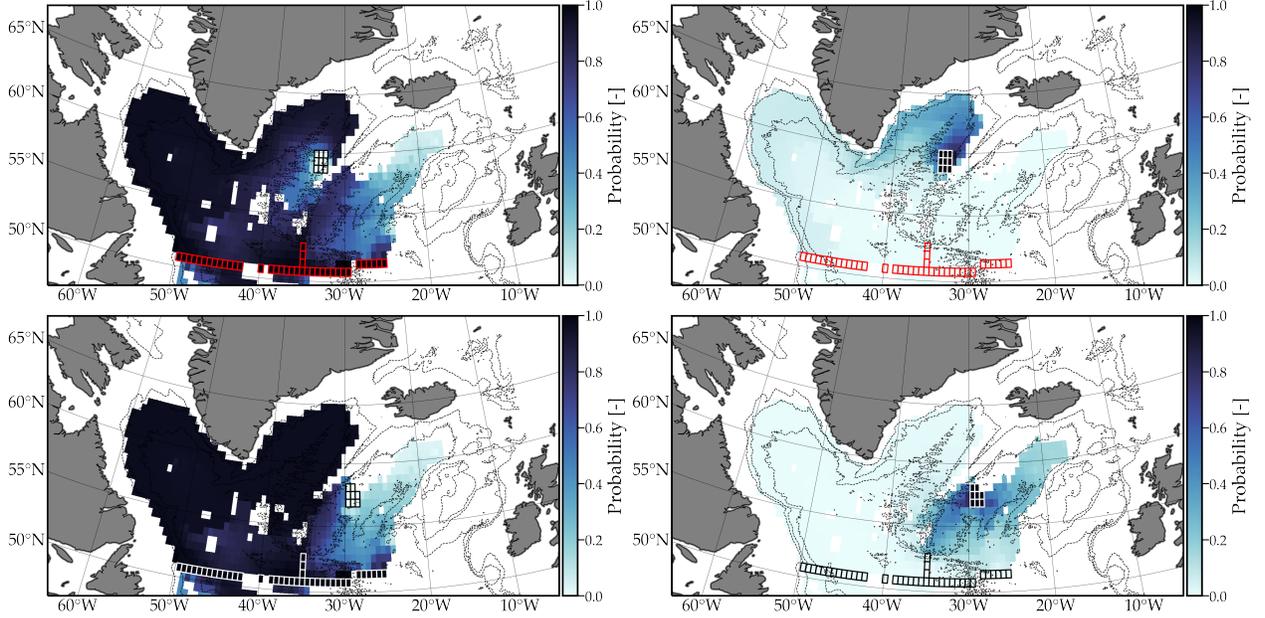

Figure 6: (top) For the LNADW Markov chain model with the source placed west of the Reykjanes Ridge, probability of trajectories to commit to the target (red boxes) in forward time (left) and to the source (black/white boxes) in backward time (right). Reactive trajectories (of UNADW) are necessarily small where the forward or backward committor probabilities are small. (bottom) As in the top panels, but with the source placed east of the Reykjanes Ridge.

The reactive currents (Fig. 7, top-left panel) and dominant transition paths (Fig. 7, top-right panel) of LNADW out of the source west of the Reykjanes Ridge, reveal a well-defined western DBC, in a manner akin to UNADW reactive currents and dominant transition paths out of the Irminger Sea source. The most notable difference is that TPT-inferred DBC in the Labrador Sea is composed of a single strongly defined branch, which roughly follows the 3000-m isobath in the Labrador Basin, consistent with f/h conservation. Note that UNADW transition paths reveal two branches even if the source is placed in the same location west of the Reykjanes Ridge used for the TPT analysis of the LNADW chain.

The TPT-inferred path from east of the Reykjanes Ridge, which are taken to roughly represent the spreading of Iceland–Scotland OW (Fig. 7, bottom panels), differ from the transition pathways of LNADW sourced west of the Reykjanes Ridge in both direction and intensity as determined by the probability of reaching the target, which is smaller. About 70% of the reactive currents are directed southward. Nearly 30% of this portion of the reactive paths flow toward the northward extension of the target at 35°W and the balance reaches boxes east of it toward the West European Basin, as anticipated by the analysis of the forward committor probability (Fig. 6, right panels). Some low-probability transition paths take a westward direction just before reaching the target around CGFZ and cross the subpolar North Atlantic interior to cross into the Labrador Sea and rejoin the DBC in that basin (Fig. 7, bottom panels). From the eastern to the western side of the Reykjanes Ridge, the magnitude of reactive currents decreases significantly, indicating that very few transitions connect one side of the ridge with the other. The results just described are not affected by the meridional portion of the target.
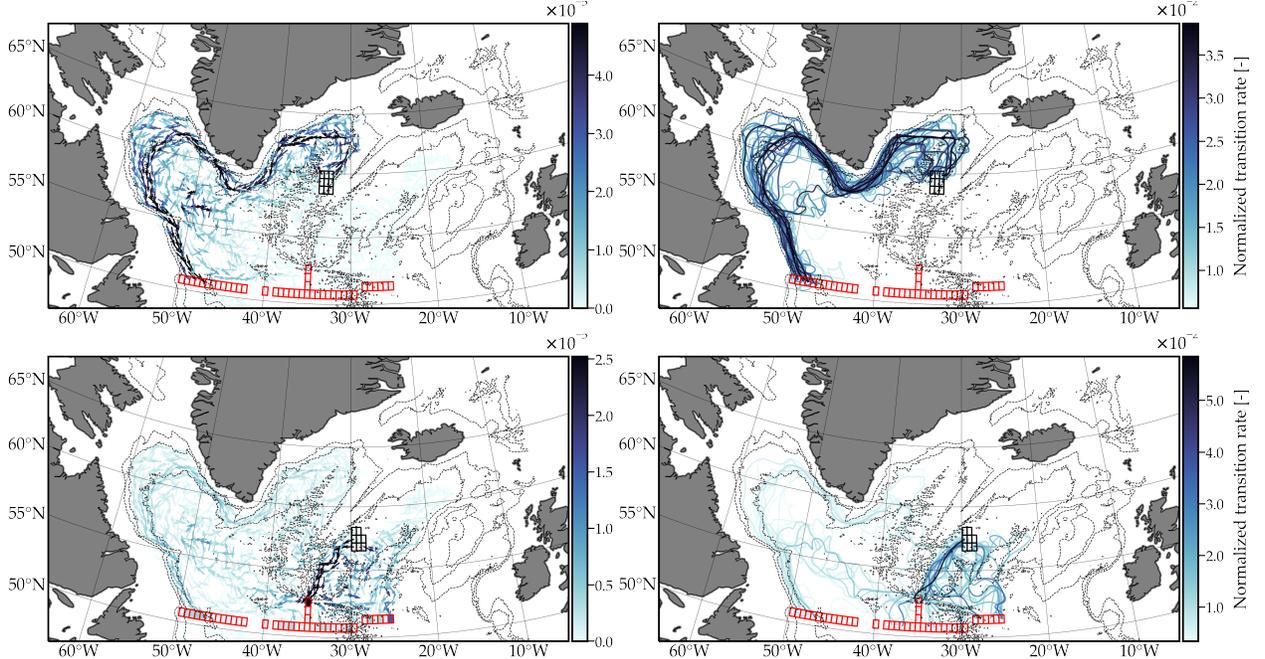
Figure 7: (top) For the LNADW chain with the source west of the Reykjanes Ridge, effective reactive currents (left) and dominant transition paths accounting for 90% of the probability flux of reactive trajectories (right). (bottom) As in the top panels, but with the source east of the Reykjanes Ridge.

We note that transition paths for LNADW resemble those for UNADW when the TPT analysis of LNADW uses UNADW sources. The only difference if that a two-branch DBC is not so well revealed, likely because of insufficient data coverage. Transition paths for UNADW with LNADW sources reveal much more organization, with the development of a quite well-defined DBC around the Reykjanes Ridge, and eventually a DBC with the separation into two branches and the subsequent merging as described above.

3.3 Mean circulation

It is valid to ask if the simple analysis of the mean Eulerian flow field, could reveal the same characteristics of the NADW paths. Figure 8 shows the mean velocity fields obtained by averaging the float velocities in the UNADW (left) and LNADW (right) layers within each box of the corresponding domain. Deducing the pathways previously identified by TPT seems hard, particularly the interior pathways since the mean Eulerian velocities away from the western boundary are negligibly small. This is consistent with the assessment by Miron et al. (2019a), who analyzed the possibility that the assumption of time homogeneity of the statistics involved in constructing their deep-flow Markov chain model, similar to those underlying the TPT analysis here, could be thought to be represented simply by advection by the mean circulation with the addition of (eddy) diffusion. Substantial differences were found, mainly because their Markov chain model, while time homogeneous, was derived from trajectories sustained by time-varying deep-ocean currents and represent, in a statistical sense, the advection–diffusion dynamics of such a *time-dependent flow*. Here we add that even if the velocity data were known with infinite resolution, the TPT trajectories can never be expected to resemble flow *trajectories*, because they actually highlight the most effective of all such trajectories connecting predefined source and target locations, i.e., they do not account for unproductive detours.

3.4 Reactive rates of UNADW and LNADW

To further quantify the distribution of transition pathways along the target, Fig. 9 presents reactive rates entering each target box from the various source, i.e., $k^{b_i \leftarrow}$ for each $b_i \subset B$, normalized by the total reactive rate into it, i.e., $k^{B \leftarrow} = \sum_{i \in B} k^{b_i \leftarrow}$, for UNADW and LNADW from the various sources considered. The results are shown as a function of longitude along the zonal piece of the target (left panel) and of latitude along its meridional piece at 35°N (right panel).
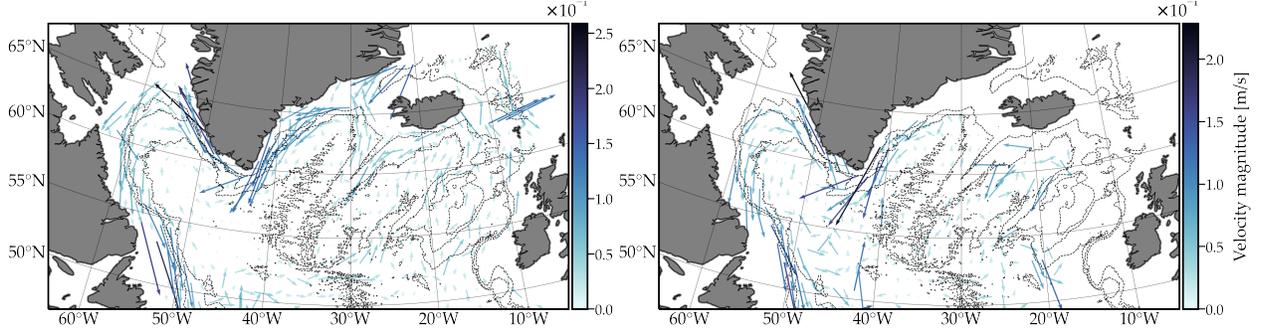
Figure 8: Mean Eulerian velocities obtained by averaging float velocities in UNADW (left) and LNADW (right) layers within each box of the domain.

The reactive rates into the latitudinal boxes of the target reveal a jet-like structure west of 45°W, for UNADW and LNADW irrespective of the source. In fact, about 79% (82%) of the reactive currents of UNADW out of the source in the Labrador (Irminger) Sea reach the target west of 45°W. For the LNADW, roughly 94% and 19% of the currents reach the target west of 45°W respectively for the LNADW chain sources east and west of the Reykjanes Ridge.

The reactive rates of UNADW (Labrador and Irminger Seas) present respectively 11% and 10% of interior pathways between 35° to 45°W. For the LNADW with the source west of the Reykjanes Ridge, internal pathways account for a mere 5% of the direct connections. The story is quite different for LNADW with the source east of the Reykjanes Ridge, for which more than 70% of the pathways to the target materialize outside of the western boundary current with a large peak around 25°W along with smaller peaks in several location west of it.

Furthermore, a nonnegligible amount of UNADW reactive rate, about 10% from the Labrador Sea source and 8.5%from the southwestern Irminger Sea source, reach the meridional set of boxes of the target concentrated at 52°N. This is consistent with inferences of zonal transport of the UNADW by Gonçalves Neto et al. (2020). For LNADW with the source east of the Reykjanes Ridge, nearly 30%reach the meridional target with a maximum around 52.5°N. This maximum is most likely due to pathways reaching the area around the CGFZ but we do not expect important westward crossing through the fracture zone since eastward transport was shown in Bower and von Appen (2008) and more recently in Gonçalves Neto et al. (2020). Nonetheless, Bower and von Appen (2008) pointed out that westbound crossings occur north of the CGFZ at 53°N and more frequently between 55° to 58°N.

These reactive rate calculations are consistent with the results from the inspection of the reactive currents and dominant paths that the route of NADW out the subpolar North Atlantic is predominantly in the form of a well-defined DBC. The UNADW reactive rates into the meridional target, albeit small, indicate transition paths from the western to the eastern subpolar North Atlantic through the CGFZ.
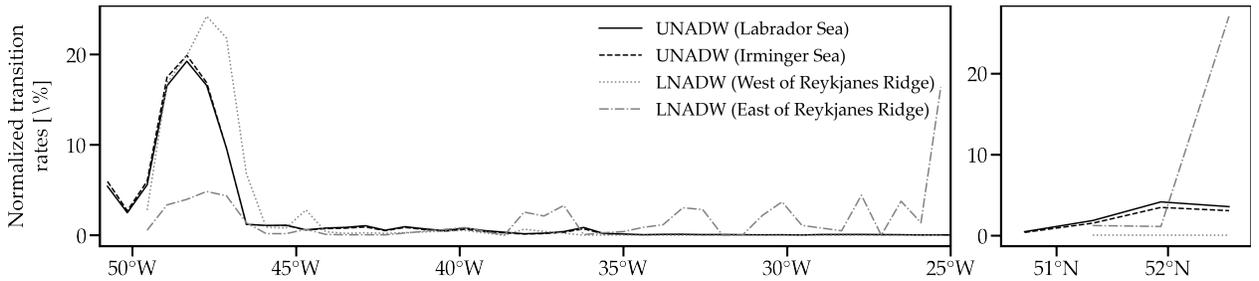

Figure 9: Reactive rates into each latitudinal (left) and meridional (right) box of the target(s) normalized by total reactive rate, for UNADW and LNADW with the source location as indicated in parenthesis.

3.5 Dynamical decomposition of the domain

The flow domain decomposition in Fig. 10, called a *forward-committor-based dynamical geography* (Miron et al., 2021), offers further insight into the NADW Lagrangian dynamics. This is accomplished as follows.

First, we place the source in the virtual two-way nirvana set (ω) used to close the system (8), in this case in such a way that probability imbalance is sent back to the chain uniformly. Since the reactive trajectories emerging from ω will necessarily have to travel through the boxes of the domain on their way to the target (B), TPT will unveil transition paths into B in the southern edge of the flow domain D *without the restriction of emerging from preset source sets.* Second, we split the target B at the southern edge of the domain into four subsets, three of them composed of zonal boxes along it, spanning nearly equally long longitudinal bands, and the fourth one comprised of its meridional boxes. Finally, the domain boxes are divided into four groups according to the maximum probability of each box to forward committing to each of the four subtargets defined above, i.e., according to whichever target is most likely to be reached from a particular grid box. Each group is colored according to the color assigned to the subtarget to which it most probably forward commits. The dynamical geography so constructed is formed by provinces analogous to backward-time basins of attraction (Miron et al., 2017, 2019a), which constrain the transport of UNADW and LNADW into the corresponding (sub)target.

More precisely, for UNADW (Fig. 10, left panel) reactive pathways from almost all boxes of the domain converge toward the westernmost subtarget (blue). The remaining subtargets (cyan, red, and magenta) are reached by transition channels emerging from regions in their close vicinity. Unlike the UNADW, which roughly shows a single dynamical province, the LNADW geography (Fig. 10, right panel) includes two large provinces (blue and magenta) separated by the Reykjanes Ridge. The red and cyan subtargets are seen to present an even smaller influence on the LNADW reactive flow dynamics than similarly located targets on that of UNADW. For both UNADW and LNADW, interior easterly reactive trajectories reach the red and cyan targets, from regions located west of the Mid-Atlantic Ridge.
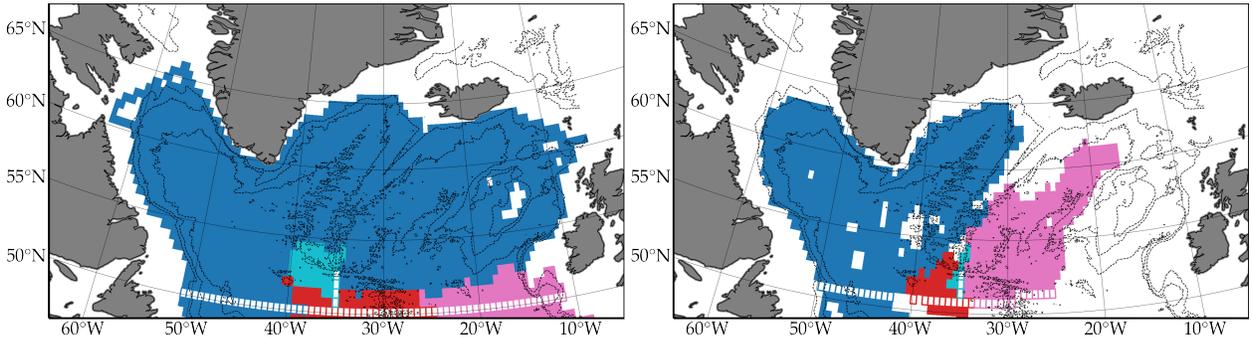

Figure 10: Decomposition of the flow domain according to the maximal probability of reactive trajectories sourced from a virtual box outside the flow domain to forward committing to each of the four subtargets into which the target in the previous figures has been split, both for the UNADW (left) and LNADW (right) chains.

3.6 Expected durations of reactive NADW pathways

Finally, Fig. 11 presents expected duration $t^{b_i B}$ of travel of reactive trajectories [cf. eq. (7)] out of *each* box b_i to the target B at the southern edge of the subpolar North Atlantic. As in the sections prior to the last one, we consider the southern border of the subpolar North Atlantic as a single target, and transitions are restricted to happen within the physical flow domain. For UNADW (Fig. 11, left panel), $t^{b_i B}$ is minimized along the western boundary of the domain (2–3 years), and clearly very close to the target, where it vanishes. Toward the east–northeast past the Reykjanes Ridge, $t^{b_i B}$ increases, reaching around 8 years. This is suggestive of cyclonic recirculation and longer direct pathways exiting the subpolar North Atlantic. For LNADW (Fig. 11, right panel), the Reykjanes Ridge has a larger impact on the circulation. From the Iceland Basin, east of the Reykjanes Ridge, the pathways reach the target about 3–5 years faster than from the Irminger Basin, west of the Ridge. This is consistent with direct visualization of multiple paths of RAFOS floats at the southern end of the Reykjanes Ridge (Zou et al., 2017). Similarly to UNADW, the expected transition time from the Labrador Sea to the target is estimated between 2–3 years along the western boundary. These results

are consistent with previous pCFC-11 age estimates in the North Atlantic as computed from observations of CFCs in the North Atlantic (Fine, 2011).
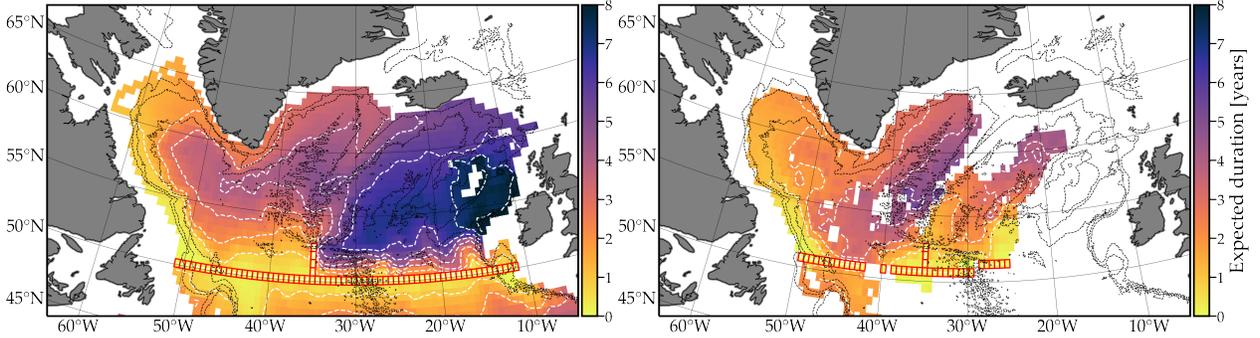

Figure 11: Mean duration of the pathways calculated from boxes of the domain to the target (red boxes) located at 50° to 51°N for the UNADW (left) and LNADW (right).

4 Discussion

A discussion of the present results in connection with earlier (Talley and McCartney, 1982) and more recent (Lozier et al., 2019; Zou et al., 2020; Georgiou et al., 2021; Koelling et al., 2021) results follows.

Using potential vorticity as a tracer, Talley and McCartney (1982) have concluded that the advection of UNADW (Labrador Sea Water) is accomplished along three main directions: northeastward into the Irminger Sea, southeastward across the North Atlantic, and southward along the Labrador Current. We observed an important recirculation toward the Irminger basin as well as a dominant southward advection along a DBC. The northeastward transport of the UNADW is not so well captured by the TPT analysis, but this may be explained by two main differences with the analysis of Talley and McCartney (1982). First, here we considered observations in the range 750–1500 m to represent UNADW, while Talley and McCartney (1982) considered depths between 500 and 2000 m. At shallower depths, between 100 and 1000 m, inspection of RAFOS floats by Bower and von Appen (2008) suggested an eastward flow between 45 and 53°N. Second, the target of our TPT analysis is positioned north of the location where Talley and McCartney (1982) observed transport extending to the east towards the Mid-Atlantic Ridge, which is influenced by the meandering of the northeastward Gulf Stream Extension/North Atlantic Current.

Our expected duration estimates appear to overestimate the transit time of deep water in the North Atlantic compared to transit time estimates by other authors. For example, Pickart et al. (2003) estimated a transit time out of the subpolar region from the Labrador Sea of about 1 year. On the other hand, Georgiou et al. (2021) estimated that transit times between 0.5 and 2 years from the Cape Farewell to 53°N from Lagrangian particle tracking using global circulation model output. Since the expected duration represents an average transit time of reactive trajectories (direct connections between source and target), the noted differences are not unexpected. Indeed, the expected duration along the DBC can be anticipated to be shorter, but interior pathways have been suggested to last within the region for over 6 years (Georgiou et al., 2021). As pointed out by these authors, the internal pathways contribute to the variability of the Atlantic meridional overturning circulation. Quantify their effects is beyond the scope of the TPT analysis in its current setting. A recent extension thereof, which introduces an explicit probability flow decomposition into direct transitions and loops supported on cycles, may provide means for doing it (Banisch et al., 2015; Helfmann et al., 2021).

The seasonal and interannual variabilities suggested by the measurements taken during the OSNAP Program (Lozier et al., 2019) cannot be quantified by the present analysis, which relies on a time homogeneity assumption. The extracted pathways of the LNADW show a higher connection outside of the WBC, as observed by Koelling et al. (2021). This might explain the disconnection pointed out by Lozier et al. (2019) between water formation from deep water sources and export outside of the subpolar region. In accordance with the results presented here, Koelling et al. (2021) also indicate a longer residence time of internal pathways and a rapid export of UNADW through the WDBC.

In turn, from the analysis of a subset of the RAFOS trajectories considered here and the aid of simulated trajectories, Zou et al. (2020) redrew the pathways of LNADW coming from the CGFZ. Rather than turning northward along the western flank of the Reykjanes Ridge, most of the LANDW was inferred to follow a

west-northwestward path or travel equatorward along the western flank of the Mid-Atlantic Ridge. A similar picture was drew by Johns et al. (2021) from the compilation of earlier results by others from float data and simulations, and from the analysis of moored current meter observations. The main difference was that they inferred a southward flows along the eastern flank of the Mid-Atlantic Ridge. These inferences are only partially in agreement with our results. The main agreement regards the west-northwestward, which TPT confirms. The major discrepancies are two. First, TPT does not discard a turning northward along the western flank of the Reykjanes Ridge (Johns et al. (2021) does not excludes this path; actually, they suggest one through the Bight Fracture Zone, which TPT also highlights). Second, TPT unveils several equatorward routes. These include: a nonnegligible WDBC (produced by the turning northward along the western flank of the Reykjanes Ridge), several southward routes west of the Mid-Atlantic Ridge, and a prominent southward path along the eastern flank of the Mid-Atlantic Ridge (Fig. 9).

5 Summary and conclusions

Several aspects of the circulation of North Atlantic Deep Water (NADW) have been quantified by applying a recent adaptation to open dynamical systems of Transition Path Theory (TPT) on available RAFOS and Argo float trajectories. TPT was developed to statistically characterize ensembles of so-called reactive trajectories. Such trajectories transition directly from a source to a target, i.e., they do not include trajectory detours that unproductively contribute to transport. We used this characteristic of reactive trajectories to unveil most effective equatorward routes for NADW within the subpolar North Atlantic. The modeling framework of TPT analysis is given by a Markov chain, under the assumption of advection–diffusion dynamics.

Two Markov chain models were constructed by discretizing the Lagrangian dynamics as described by the float trajectories. One chain involved floats at parking depths in the 750–1500-m range to represent the upper layer of NADW (UNADW), mainly comprised of Labrador water. The other chain used floats with parking depth ranging between 1800 and 3500 m, representative of the lower layer of NADW (LNADW) mainly comprised of Overflow Water. Preset sources of UNADW in the Labrador and southwestern Irminger Seas, and of LNADW west and east of the Reykjanes Ridge were considered in the TPT analysis. The target was located along 50°N, taken to represent the southern edge of the subpolar North Atlantic to within the limits imposed by the availability of data and the depth of the water masses.

The UNADW component of the TPT-inferred DBC was found to flow between the 2000- and 3000-m isobaths, while showing two branches in the Labrador Sea where those isobaths diverge. Each branch follows each of these isobaths closely. Interior paths of UNADW through the Charlie–Gibbs Zone were also unveiled, but amounting to a reduced fraction, not exceeding 20%, of the total UNADW transitions. The majority of the LNADW transition paths (95%) tracked out of a source west of the Reykjanes Ridge were found to form a DBC, well organized roughly along the 3000-m isobath. LNADW tracked out from a source east of the Reykjanes Ridge revealed a lesser degree of organization. About 20% of the transitions organized along a DBC, while nearly 30% converged east of the Mid-Atlantic Ridge on the target at the southern edge of the domain. The rest of the transitions hit the target in several places distributed along thereof, indicating southward flow along the western flank of the Mid-Atlantic Ridge as well. A source-independent dynamical decomposition of the flow domain into analogous backward-time basins of attraction consistently reveal a much wider influence of the western side of the target for UNADW than for LNADW. The former spans nearly the entire subpolar North Atlantic, while the latter is confined to the Labrador and Irminger Seas. For UNADW, the average expected duration of the pathways from the Labrador and Irminger Seas was found to range between 2 and 3 years. For LNADW, the expected duration of the pathways was found to be largely influenced by the Reykjanes Ridge. This found to be as long as 8 years for paths sourced on the western side of the ridge, while of about 3 years on average for those on its eastern side.

Future work should aim to expand spatiotemporal coverage and consider isopycnal ranges, which, unlike fixed depth ranges, most naturally constrain UNADW and LNADW. Clearly, both are beyond reach of existing observational platforms, so one will necessarily have to resort to numerical simulation. At a much more fundamental level lies the question of the extent to which float motion represents fluid motion, which can be studied using recent results on the dynamics of inertial (i.e., buoyant, finite-size) particles (Beron-Vera et al., 2015). Addressing these questions is left for the future.

Acknowledgments

Data availability statement

The RAFOS float data are distributed by the National Oceanic and Atmospheric Administration's (NOAA) Atlantic Oceanographic and Meteorological Laboratory (AOML) through the subsurface data sets website at `https://www.aoml.noaa.gov/phod/float_traj/`. The trajectories of the Argo floats at their parking level are available in near-real time at `http://apdrc.soest.hawaii.edu/projects/yomaha` (Lebedev et al., 2007). Finally, the numerical code used in this study is publicly available at `https://github.com/philippemiron/pygtm`.

References

Banisch, R., N. D. Conrad, and C. Schütte, 2015: Reactive flows and unproductive cycles for random walks on complex networks. *The European Physical Journal Special Topics*, **224 (12)**, 2369–2387.

Beron-Vera, F. J., N. Bodnariuk, M. Saraceno, M. J. Olascoaga, and C. Simionato, 2020: Stability of the Malvinas Current. *Chaos: An Interdisciplinary Journal of Nonlinear Science*, **30 (1)**, 13 152, doi: 10.1063/1.5129441.

Beron-Vera, F. J., M. J. Olascoaga, G. Haller, M. Farazmand, J. Triñanes, and Y. Wang, 2015: Dissipative inertial transport patterns near coherent Lagrangian eddies in the ocean. *Chaos*, **25 (8)**, 1–12, doi:10. 1063/1.4928693, 1408.6512.

Bower, A., and Coauthors, 2019: Lagrangian Views of the Pathways of the Atlantic Meridional Overturning Circulation. *Journal of Geophysical Research: Oceans*, **124 (8)**, 5313–5335, doi:10.1029/2019JC015014.

Bower, A. S., M. S. Lozier, S. F. Gary, and C. W. Böning, 2009: Interior pathways of the North Atlantic meridional overturning circulation. *Nature*, **459 (7244)**, 243–247.

Bower, A. S., and W.-J. von Appen, 2008: Interannual variability in the pathways of the North Atlantic Current over the Mid-Atlantic Ridge and the impact of topography. *Journal of Physical Oceanography*, **38 (1)**, 104–120.

Brémaud, P., and J. R. Norris, 1975: *Markov chains*, Gibbs Fields Monte Carlo Simulation Queues, Texts in Applied Mathematics, Vol. 19. Cambridge University Press, New York, 91–121 pp., doi: 10.1016/S0070-4571(08)70371-6.

Cuny, J., P. B. Rhines, P. P. Niiler, and S. Bacon, 2016: Labrador Sea Boundary Currents and the Fate of the Irminger Sea Water. *Journal of Physical Oceanography*, **32**, 627–647.

de Jong, M. J., A. S. Bower, and H. H. Furey, 2016: Seasonal and Interannual Variations of Irminger Ring Formation and Boundary–Interior Heat Exchange in FLAME. *Journal of Physical Oceanography*, **46**, 1717–1734.

Drouin, K. L., M. Susan Lozier, F. J. Beron-Vera, P. Miron, and M. J. Olascoaga, 2012: Surface pathways connecting the South and North Atlantic Oceans. *Geophysical Research Letters*, **49**, e2021GL096 646, doi:10.1029/2021GL096646.

E, W., and E. Vanden-Eijnden, 2006: Towards a theory of transition paths. *Journal of statistical physics*, **123 (3)**, 503–523.

E, W., and E. Vanden-Eijnden, 2010: Transition-path theory and path-finding algorithms for the study of rare events. *Annual Review of Physical Chemistry*, **61**, 391–420, doi:10.1146/annurev.physchem.040808.090412.

Fine, R. A., 2011: Observations of CFCs and SF6 as ocean tracers. *Annual Review of Marine Science*, **3**, 173–195.

Fischer, J., and F. A. Schott, 2002: Labrador Sea Water tracked by profiling floats—From the boundary current into the open North Atlantic. *Journal of Physical Oceanography*, **32 (2)**, 573–584.

Froyland, G., P. K. Pollett, and R. M. Stuart, 2014: A closing scheme for finding almost-invariant sets in open dynamical systems. *Journal of Computational Dynamics*, **1 (1)**, 135–162, doi:10.3934/jcd.2014.1.135.

Georgiou, S., S. L. Ypma, N. Brüggemann, J.-M. Sayol, C. G. van der Boog, P. Spence, J. D. Pietrzak, and C. A. Katsman, 2021: Direct and indirect pathways of convected water masses and their impacts on the overturning dynamics of the Labrador Sea. *Journal of Geophysical Research: Oceans*, **126 (1)**, e2020JC016 654.

Gonçalves Neto, A., J. B. Palter, A. Bower, H. Furey, and X. Xu, 2020: Labrador Sea Water Transport Across the Charlie-Gibbs Fracture Zone. *Journal of Geophysical Research: Oceans*, **125 (8)**, e2020JC016 068, doi: 10.1029/2020JC016068.

Helfmann, L., 2020: Extending Transition Path Theory for Time-Dependent Dynamics. Ph.D. thesis, Free University of Berlin.

Helfmann, L., J. Heitzig, P. Koltai, J. Kurths, and C. Schütte, 2021: Statistical analysis of tipping pathways in agent-based models. *European Physical Journal: Special Topics*, **230 (16-17)**, 3249–3271, doi:10.1140/epjs/s11734-021-00191-0, URL https://doi.org/10.1140/epjs/s11734-021-00191-0, 2103.02883.

Johns, W. E., M. Devana, A. Houk, and S. Zou, 2021: Moored Observations of the Iceland-Scotland Overflow Plume Along the Eastern Flank of the Reykjanes Ridge. *Journal of Geophysical Research*, **126**, e2021JC017 524.

Koelling, J., D. Atamanchuk, J. Karstensen, P. Handmann, and D. W. R. Wallace, 2021: Oxygen export to the deep ocean following Labrador Sea Water formation. *Biogeosciences Discussions*, 1–25.

LaCasce, J. H., and A. Bower, 2000: Relative dispersion in the subsurface north atlantic. *Journal of Marine Research*, **58 (6)**, 863–894, doi:10.1357/002224000763485737, URL http://www.ingentaselect.com/rpsv/cgi-bin/cgi?ini=xref&body=linker&reqdoi=10.1357/002224000763485737.

Lavender, K. L., R. E. Davis, and W. B. Owens, 2000: Direct velocity measurements in the Labrador and Irminger Seas describe pathways of Labrador Sea Water. *Nature*, **407**, 66–69.

Lavender, K. L., W. B. Owens, and R. E. Davis, 2005: The mid-depth circulation of the subpolar North Atlantic Ocean as measured by subsurface floats. *Deep Sea Research Part I: Oceanographic Research Papers*, **52 (5)**, 767–785.

Lebedev, K. V., H. Yoshinari, N. A. Maximenko, and P. W. Hacker, 2007: YoMaHa'07: Velocity data assessed from trajectories of Argo floats at parking level and at the sea surface. *IPRC Technical Note*, **2 (4)**, 20.

Lozier, M. S., S. F. Gary, and A. S. Bower, 2013: Simulated pathways of the overflow waters in the North Atlantic: Subpolar to subtropical export. *Deep Sea Research Part II: Topical Studies in Oceanography*, **85**, 147–153.

Lozier, M. S., and Coauthors, 2019: A sea change in our view of overturning in the subpolar North Atlantic. *Science*, **363 (6426)**, 516–521, doi:10.1126/science.aau6592.

Maximenko, N., J. Hafner, and P. Niiler, 2012: Pathways of marine debris derived from trajectories of Lagrangian drifters. *Marine Pollution Bulletin*, **65 (1-3)**, 51–62, doi:10.1016/j.marpolbul.2011.04.016, URL http://dx.doi.org/10.1016/j.marpolbul.2011.04.016.

Metzner, P., C. Schütte, and E. Vanden-Eijnden, 2006: Illustration of transition path theory on a collection of simple examples. *Journal of Chemical Physics*, **125 (8)**, 84 110, doi:10.1063/1.2335447.

Metzner, P., C. Schütte, and E. Vanden-Eijnden, 2009: Transition Path Theory for Markov Jump Processes. *Multiscale Modeling & Simulation*, **7 (3)**, 1192–1219, doi:10.1137/070699500.

Miron, P., F. J. Beron-Vera, L. Helfmann, and P. Koltai, 2021: Transition paths of marine debris and the stability of the garbage patches. *Chaos: An Interdisciplinary Journal of Nonlinear Science*, **31 (3)**, 033 101, doi:10.1063/5.0030535.

Miron, P., F. J. Beron-Vera, M. J. Olascoaga, G. Froyland, P. Pérez-Brunius, and J. Sheinbaum, 2019a: Lagrangian geography of the deep gulf of mexico. *Journal of Physical Oceanography*, **49 (1)**, 269–290, doi:10.1175/JPO-D-18-0073.1, 1804.06843.

Miron, P., F. J. Beron-Vera, M. J. Olascoaga, and P. Koltai, 2019b: Markov-chain-inspired search for MH370. *Chaos*, **29 (4)**, doi:10.1063/1.5092132, 1903.06165.

Miron, P., F. J. Beron-Vera, M. J. Olascoaga, J. Sheinbaum, P. Pérez-Brunius, and G. Froyland, 2017: Lagrangian dynamical geography of the Gulf of Mexico. *Scientific Reports*, **7 (1)**, doi:10.1038/s41598-017-07177-w, URL https://doi.org/10.1038/s41598-017-07177-w, 1703.10684.

Olascoaga, M. J., P. Miron, C. Paris, P. Pérez-Brunius, R. Pérez-Portela, R. H. Smith, and A. Vaz, 2018: Connectivity of Pulley Ridge With Remote Locations as Inferred From Satellite-Tracked Drifter Trajectories. *Journal of Geophysical Research: Oceans*, **123 (8)**, 5742–5750, doi:10.1029/2018JC014057.

Pickart, R. S., F. Straneo, and G. W. K. Moore, 2003: Is Labrador Sea water formed in the Irminger basin? *Deep Sea Research Part I: Oceanographic Research Papers*, **50 (1)**, 23–52.

Ramsey, A. L., H. H. Furey, and A. S. Bower, 2020: Overturning of the Subpolar North Atlantic Program (OSNAP): RAFOS Float Data Report June 2014 - January 2019. Tech. rep., Woods Hole Oceanographic Institution. doi:10.1575/1912/26515.

Sabine, C. L., and T. Tanhua, 2010: Estimation of anthropogenic CO2 inventories in the ocean. *Annual review of marine science*, **2**, 175–198.

Stommel, H., 1958: The abyssal circulation. *Deep-Sea Res.*, **5**, 80–82.

Susan Lozier, M., and Coauthors, 2017: Overturning in the Subpolar North Atlantic Program: A new international ocean observing system. *Bulletin of the American Meteorological Society*, **98 (4)**, 737–752.

Talley, L. D., and M. S. McCartney, 1982: Distribution and circulation of Labrador Sea water. *Journal of Physical Oceanography*, **12 (11)**, 1189–1205.

Vanden-Eijnden, E., 2006: Transition path theory. *Computer Simulations in Condensed Matter Systems: From Materials to Chemical Biology Volume 1*, Springer, 453–493.

Zou, S., A. Bower, H. Furey, M. S. Lozier, and X. Xu, 2020: Redrawing the Iceland- Scotland Overflow Water pathways in the North Atlantic. *Nature communications*, **11 (1)**, 1–8.

Zou, S., S. Lozier, W. Zenk, A. Bower, and W. Johns, 2017: Observed and modeled pathways of the Iceland Scotland Overflow Water in the eastern North Atlantic. *Progress in Oceanography*, **159**, 211–222.